


Article

Effect of Curing Regime on the Mechanical Properties and Durability of Steam Cured-Concrete

Ling Wang, Wenzhu Wei, Junfei Zhang , Yuanchen Hu and Lei Zhang *

School of Civil and Transportation Engineering, Hebei University of Technology, 5340 Xiping Road, Tianjin 300401, China

* Correspondence: lzhan666@hebut.edu.cn

Abstract: The application of pre-cast components in building structures has become increasingly widespread, with projects often utilizing steam curing methods. The utilization of pre-fabricated concrete has demonstrated the capacity to enhance construction efficiency. However, strength and durability issues arising from steam curing of concrete have become prominent considering the quality of concrete construction. The use of fly ash and slag in steam-cured concrete to improve its performance has gained extensive popularity. While research into single-blended mineral admixtures has been conducted with notable achievements, the study of steam-cured concrete with binary blended mineral admixtures remains relatively limited. This paper focuses on the mechanical properties and durability of steam-cured concrete with mineral admixtures (fly ash and slag), exploring the influence of mineral admixture ratios and steam-curing regimes on the mechanical properties and durability of concrete. The properties of the steam-cured concrete were further analyzed through compressive strength tests, mercury intrusion porosimetry, and thermogravimetric analyses. It was found that when fly ash and slag were added in equal proportions, the compressive strength and microstructure of the concrete were optimized. In addition, the optimized static resting time and constant temperature time should be controlled as 3 h and 6 h, respectively, to improve the compressive strength and microstructure of the steam-cured concrete.

Keywords: steam-cured concrete; minerals; compressive strength; microstructure; durability

Citation: Wang, L.; Wei, W.; Zhang, J.; Hu, Y.; Zhang, L. Effect of Curing Regime on the Mechanical Properties and Durability of Steam Cured-Concrete. *Buildings* **2023**, *13*, 1697. <https://doi.org/10.3390/buildings13071697>

Academic Editor: Giuseppina Uva

Received: 17 May 2023

Revised: 20 June 2023

Accepted: 26 June 2023

Published: 3 July 2023



Copyright: © 2023 by the authors. Licensee MDPI, Basel, Switzerland. This article is an open access article distributed under the terms and conditions of the Creative Commons Attribution (CC BY) license (<https://creativecommons.org/licenses/by/4.0/>).

1. Introduction

Global warming has been a grave concern since the pre-industrial era, mainly due to the continuous release of carbon dioxide emissions [1,2]. It has been reported that buildings account for 36% of global energy consumption, and the construction industry contributes to 39% of the global greenhouse gas emissions [3]. Consequently, there is a pressing need to reduce building energy consumption and carbon dioxide emissions, which has spurred research in energy-saving and decarbonizing renovations in the building sector [4]. Pre-fabricated construction is a sustainable and efficient technology that has been introduced in China over the past few decades. It has shown promising results in mitigating carbon dioxide emissions [5,6]. For example, Cao et al. [7] stated that a 35.82% decrease in resource depletion was achieved in pre-fabricated construction compared to conventional on-site construction. Furthermore, a study by Hong et al. [8] demonstrated that adopting pre-fabricated construction could save 4–14% of total life-cycle energy consumption. Apart from its environmental benefits, pre-fabricated construction offers advantages in terms of quality control [9], production efficiency, shorter operation times, and lower labor demand compared to traditional construction modes. To sum up, these findings indicate that pre-fabricated construction could be an effective strategy for achieving energy-saving and decarbonization goals in the building sector, while also improving the quality and efficiency of construction.

To accelerate curing, various methods have been used in the production of pre-fabricated concrete units, such as steam curing [10], electric thermal curing, microwave

curing, infrared curing, etc. Among these, steam curing is most widely used in China owing to its ease of operation [11]. According to statistical data, a majority of manufacturers in China (more than 70%) employ steam curing as the primary accelerating curing method. A typical steam curing process includes a delay period after surface finishing, a heating–cooling cycle with a rate of 11–44 °C/h, and a period of 6–18 h with a constant temperature typically resting at 60–90 °C [12–14]. Steam curing plays a pivotal role in accelerating pre-fabrication construction by shortening the demolding time, expediting the strength gain, and supplying the necessary heat for concrete hydration. Through the implementation of steam curing, a pre-fabricated concrete component can attain 70% of its standard design strength within a mere 24 h [15].

However, owing to the loss of interior moisture content and the heterogeneous distribution of the hydration products, steam curing causes a series of adverse effects, such as pronounced volumetric deformation and shrinkage [16–19], surface micro-cracking [16,20], pore structure coarsening [21–24], and long-term mechanical and durability issues [21,25–29]. Considerable research efforts have been devoted to investigating the adverse effects of steam-curing and their underlying mechanisms. For example, He et al. [30] stated that the deterioration of concrete after steam curing could be attributed to the high temperature. Therefore, they defined the adverse effects of steam curing on concrete as “heat damage”. Similarly, Gallucci et al. [31] undertook an in-depth exploration of the temperature-induced alterations in calcium–silicate–hydrate (C-S-H). Their findings revealed that the apparent density of C-S-H showed a persistent rise from the nanoscale with an increase in the curing temperature. Consequently, the microstructure of the cement paste exhibited a more porous and coarse configuration. In addition, the final extent of hydration remains unaffected by changes in temperature. Shi et al. [32] concluded that higher treatment temperatures during steam curing led to more intricate temperature-humidity gradients, resulting in a concrete microstructure characterized by reduced compactness and heightened permeability.

Various mitigation strategies, including the optimization of the steam curing regime [32–34], incorporation of mineral admixtures [26,35,36], and implementation of internal curing techniques [37], have been reported in the literature to ameliorate the adverse effects of steam curing on concrete. Adding mineral admixtures, such as fly ash or slag, as a substitute for cement in steam-cured concrete can improve its adaptability to the curing conditions [35,38]. Additionally, the inclusion of mineral admixtures in concrete induces a delay in the hydration process of the cementitious component, thus having a positive effect in terms of mitigating heat damage [39]. Notably, the addition of mineral admixtures to concrete during steam curing can improve its long-term strength, which is beneficial for enhancing the durability of steam-cured concrete [40].

Considerable interest has been directed, in recent years, toward the use of mineral admixtures in steam-cured concrete. For example, Ho et al. [26] investigated the potential advantages of incorporating different mineral admixtures, such as fly ash, slag, and silica fume, into steam-cured concrete. The findings revealed that, despite the inclusion of these admixtures, the steam-cured concrete exhibited higher porosity compared to specimens cured under standard conditions. Notably, the mixes incorporating silica fume demonstrated superior performance, exhibiting remarkable prospects in pre-cast manufacturing due to their exceptional ex-steam compressive strength and low sorptivity values. Wang et al. [19] conducted a study into the volume deformation of fly ash concrete during the early stages of steam curing. Their findings demonstrate that autogenous shrinkage occurred during the constant temperature phase of steam curing, while post-curing shrinkage primarily arose from the drying effect. Incorporating fly ash into the concrete mixture accelerated shrinkage evolution during the steam curing process, though it proved advantageous for post-curing shrinkage mitigation. Ramezani-pour et al. [41] investigated the effect of steam curing and various types of mineral admixtures (metakaolin, pomis, and trass) on the mechanical properties and durability of self-compacting concrete (SCC). The findings indicate that the steam-cured SCC with metakaolin showed the highest compressive strength owing to its higher pozzolanic reactivity, thus promoting early hydration.

In addition, the incorporation of mineral additives resulted in enhanced durability. This improvement can be attributed to the accelerated formation of C-S-H gel and CH crystalline phases, which effectively restricted the ingress of deleterious substances by impeding pore filling within the inner structure.

In recent years, there has been intense research into the performance of steam-cured concrete in incorporating mineral admixtures, though this research has been largely focused on a single mineral admixture. The research into the durability of steam-cured concrete with binary mineral admixture system is relatively scarce, which has practical significance for the durability design of pre-fabricated components. This study investigated the effects of binary mineral admixtures (fly ash and blast furnace slag) and steam curing conditions on the carbonation resistance, water resistance, and chloride ion permeability of steam-cured concrete. By varying the steam curing methods and the ratio of mineral admixtures, the effects of the mineral admixtures with different proportions on durability in diverse steam curing environments were examined. The findings provide valuable technical support for the applications of steam-cured concrete.

2. Materials and Methods

2.1. Materials

Ordinary Portland cement (OPC, CEM I 52.5) sourced from Laishui Jidong Co., Ltd. (Baoding City, Hebei, China) was used. Fly ash (Grade I) complied with GB 1596-91, and blast furnace slag (Grade S95) obtained from Qianjin Metallurgical Technology Co., Ltd., Shijiazhuang City, Hebei, China, was employed as the mineral admixtures. The specifications of the above admixtures are shown in Tables 1–3. The fine aggregate with a fineness modulus of 2.6, clay content of less than 1.5%, and rock fragment content of less than 1.0% was categorized as Zone II River sand. The coarse aggregate was formed of crushed gravel with clay content of less than 1% and rock fragment content of less than 0.5%, and only 3% of the particles had needle-like shapes.

Table 1. Mechanical properties of ordinary Portland cement.

Projects		Measurement Results
	Initial setting/min	185
	Final setting/min	370
	Standard consistency water consumption/mL	139
	Stability	Conformity
Flexural strength/MPa	3 day	6.0
	28 day	9.1
Compressive strength/MPa	3 day	29.9
	28 day	54.3

Table 2. Technical Indexes of grade I fly ash.

Projects	Measurement Results
Fineness (0.045 mm)/%	9.0
Burn loss/%	4.1
Water demand ratio/%	94

Table 3. Technical index of S95 grade slag.

Projects		Measurement Results
Activity index/%	7 day	87
	28 day	96
	Water content/%	0.7
	Burn loss/%	0.6

2.2. Mix Proportions and Sample Preparations

The water-to-binder ratio (W/B) was 0.37. By fixing the constant W/B, the mineral admixtures were used to replace the OPC in equal amounts. The ratios of the mineral admixtures (fly ash: slag) were 1:0, 1:0.5, 1:1, 1:2, and 0:1, respectively. The mix proportion of concrete is presented in Table 4.

Table 4. Concrete mix ratio kg/m³.

Mix Ratio Group	Cement	Fly Ash	Slag	Sand	Stones	Water	Water-Reducer
L1	280	130	0	735	1060	190	6.56
L2	280	86.7	43.3	735	1060	190	6.15
L3	280	65	65	735	1060	190	6.15
L4	280	43.3	86.7	735	1060	190	6.15
L5	280	0	130	735	1060	190	5.74

Note: adjust the amount of water-reducer to control the slump between 160 and 180 mm.

A JJ-5 planetary mixer, which was manufactured in Zhejiang, China, was employed to produce homogenous concrete. The raw materials, including coarse and fine aggregates, were pre-mixed for 1 min. OPC and mineral admixtures were then added at a low mixing speed of 165 rpm, and mixing continued at this speed for an additional minute. Afterward, water containing SP was added, and the mixing speed was increased to a medium speed of 300 rpm for 3 min.

2.3. Curing Regime

The steam-curing cycle consisted of mold loading, static resting, heating, constant temperature, and cooling. The concrete specimens were placed at room temperature for 3 h and then heated at a rate of 15 °C/h until reaching a constant temperature of 55 °C, which was maintained for 4 h. Subsequently, the specimens were removed from the curing environment and cooled at a rate of 15 °C/h until they reached room temperature. In order to investigate the influence of changes in steam curing process parameters on the durability performance of mineral admixture concrete, adjustments were made to the static resting time and constant temperature time parameters. The steam curing static resting times were set to 1, 2, 3, and 4 h, while the constant temperature times were set to 3, 4, 6, and 8 h. The steam curing system schemes and their corresponding labels are listed in Table 5.

Table 5. Steam curing system scheme.

Group	Static Resting Time (h)	Constant Temperature Time (h)
P1	1	4
P2	2	4
P3	3	4
P4	4	4
P5	3	3
P6	3	6
P7	3	8

The present study investigated the application of fly ash and slag in steam-cured concrete and examined the effects of composite proportions of the admixtures, static resting times, and constant temperature times on the compressive strength and microstructure of the concrete. The specimens were prepared based on the mix proportions presented in Table 6. The experimental procedures were devised as follows (see in Table 7):

- (1) Under the same steam curing system conditions of P3, mineral admixtures (fly ash and slag) were used to replace 32% of the cement based on mass. The replacement schemes were as follows: S1 (single fly ash replacement), S2 (fly ash and slag at a ratio of 2:1), S3 (fly ash and slag at a ratio of 1:1), S4 (fly ash and slag at a ratio of 1:2),

- and S5 (single slag replacement). The corresponding steam curing system scheme numbers range from A-1 to A-5;
- (2) Under the same mix proportion of S3 (fly ash and slag at a ratio of 1:1), the steam-curing static resting times were set to 1 h, 2 h, 3 h, and 4 h for labels B-1 to B-4;
 - (3) Under the same mix proportion of S3 (fly ash and slag at a ratio of 1:1), the constant temperature resting times were set to 3 h, 4 h, 6 h, and 8 h for labels C-1 to C-4.

Table 6. Mortar mix ratio kg/m³.

Group	Cement	Fly Ash	Slag	Sand	Water	Water-Reducer
S1	280	130	0	735	190	6.56
S2	280	86.7	43.3	735	190	6.15
S3	280	65	65	735	190	6.15
S4	280	43.3	86.7	735	190	6.15
S5	280	0	130	735	190	5.74

Table 7. Test scheme.

Group	Composite Ratio of Admixtures	Steam Curing System	Group	Mix Proportion	Static Resting Time (h)	Group	Mix Proportion	Constant Temperature Time (h)
A-1	1:0	Same steam curing system P3	B-1	Same mix ratio L3	1	C-1	Same mix ratio L3	3
A-2	1:0.5		B-2		2	C-2		4
A-3	1:1		B-3		3	C-3		6
A-4	1:2		B-4		4	C-4		8
A-5	0:1							

2.4. Experimental Methods

2.4.1. Compressive Strength Tests

In accordance with GB/T50081-2019, cubic specimens with sizes of 150 mm × 150 mm × 150 mm were prepared to conduct compressive tests. Each specimen was subjected to a consistent loading rate of 5 kN per second, and testing was conducted within an environment maintained at a temperature of approximately 22 ± 2 °C. To ensure the reliability and accuracy of experimental results, a minimum of 3 specimens were subjected to testing, with the compressive strength calculated as the mean value of measured results. The standard deviation of these values was required to be no greater than 10% in order to ensure validity.

2.4.2. Mercury Intrusion Porosimetry (MIP) Test

The cumulative pore volume of the cement paste samples was analyzed using the AutoPore IV 9500 version 2.01 instrument (Micromeritics Instruments) via the MIP technique. Prior to the MIP test, the samples, which lay within the 6–10 mm range, were immersed in acetone and subjected to a vacuum desiccator for 48 h to terminate the hydration process [42,43]. The MIP test was conducted on the samples subsequent to their removal from the desiccator. Mercury temperature was maintained at 20 °C, while the penetrometer volume was set at 6.6376 mL. The MIP test was conducted with a contact angle of 130°, in continuous mode, and with a pressure range of 0.10–61,000 psi.

2.4.3. Thermogravimetry and Differential Thermogravimetry (TG-DTG)

Thermal analysis of the sample was performed via TG-DTG on a TA SDT Q600 instrument, using a nitrogen atmosphere with a heating rate of 10 °C/min over a temperature range of 40–1000 °C. To determine the quantity of mass loss during each decomposition process, the DTG curves were deconvoluted using the Gaussian area deconvolution method, with Origin 2017 software utilized to extract the area associated with each process.

2.4.4. Rapid Chloride Migration (RCM) Test

Cylindrical concrete specimens, with each having a thickness of 50 mm, were meticulously cut and vacuum saturated for 24 h prior to undergoing chloride migration coefficient evaluation via the RCM test, as per GB/T 50082-2009. To ensure the reliability of the test results, 3 samples were utilized for each trial. Specifically, the concrete samples were securely held within rubber rings, and they were immersed in 300 mL of 0.3 mol/L NaOH solution while being placed within a plastic tank filled with a 10% weight NaCl solution. The positive electrode was then affixed to the surface of the concrete specimen in the NaOH solution, while the negative electrode was attached to the opposite side of the specimen in the NaCl solution. After testing, the specimens were cleaved in half, and the chloride penetration depth was then assessed via employment of a 0.1 mol/L AgNO₃ solution. The chloride ion diffusion coefficient of the concrete was subsequently calculated in accordance with the following formula:

$$D_{RCst} = \frac{0.0239 \times (237 + T)L}{(U - 2)t} \left(X_d - 0.0238 \sqrt{\frac{(237 + T)LX_d}{U - 2}} \right) \quad (1)$$

where, D_{RCM} is the unsteady chloride ion migration coefficient of concrete (m²/s), U is the absolute value of the applied voltage (V), T is the average temperature of the anode solution from the beginning to the end (°C), L is the specimen thickness (mm), X_d is the average value of the chloride penetration depth (mm), and t is the duration of the trial (h).

3. Results and Discussion

3.1. Compressive Strength

3.1.1. The Effect of Steam Curing and Mineral Admixtures on the Compressive Strength Compared to Standard Curing

Regarding the standard curing of the concrete, the specimens were demolded and placed in a standard curing room after molding the specimens for 24 h. The steaming curing process includes a static resting period of 3 h, a temperature rise of 15 °C/h, a constant temperature of 55 °C for 4 h, and a temperature reduction of 15 °C/h. After steaming, the specimens were demolded and placed in a standard curing room for further curing until the reaching age of 28 days. The compressive strength test was conducted after curing until reaching the age of 28 days. Figure 1 shows the 28-day compressive strength of the steam-cured concrete that incorporated minerals with varied ratios in comparison to the standard curing regime. It was found that the 28-day compressive strength of steam-cured concrete was lower than that of conventionally cured concrete. Compared to standard curing, higher steam curing temperatures promote the acceleration of the C₃S hydration phase, leading to a rapid reduction in the duration of the hydration process [44]. Higher steam curing temperatures also considerably increased the average length of the C-S-H gel chains within a shorter curing time, which rose from two chain segments to eight chain segments, thereby resulting in the higher early-age strength of the concrete. However, as the age of the concrete increased, the length of the chains no longer increased, and the C-S-H gel formed long chains over a short period, which in turn lead to non-uniform hydration product formation and a higher porosity, thereby lowering the later-age compressive strength. In contrast, concrete cured under standard conditions was continuously exposed to a high-humidity environment, which provides the concrete with the moisture necessary for the hydration reaction.

The influence of fly ash-to-slag ratios on the 28-day strength of the steam-cured concrete is also demonstrated in Figure 1. The compound with addition of the two minerals with a ratio of 1:1 achieved the highest compressive strength; however, the concrete that only incorporated fly ash showed the lowest compressive strength. For instance, after 28 days, the steam-cured concrete with fly ash and slag with a ratio of 1:1 (42.7 MPa) achieved a 17.3% increase in compressive strength compared to the concrete that only

incorporated fly ash (36.4 MPa). High-temperature curing enhanced cement hydration and produced alkaline activator $\text{Ca}(\text{OH})_2$, which stimulated the pozzolanic effect of the mineral admixtures, improved the hydration degree of the early system, and promoted the early reactivity. The highest compressive strength of the steam-cured concrete incorporating fly ash and slag was due to the synergistic effect of the compound, which increased the compactness of concrete, the secondary hydration reaction of mineral admixtures, and the improvement in the cement paste and aggregate interface area of concrete, ultimately enhancing the later strength of the concrete.

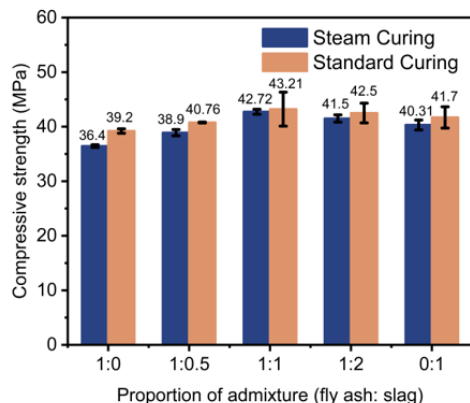


Figure 1. Effect of steam curing regime on the compressive strength of the concrete incorporating minerals.

3.1.2. The Effect of Static Resting Time on the Compressive Strength

The 1-day demolding and 28-day compressive strength values of the steam-cured concrete with varied static resting times in the presence of fly ash and slag at a 1:1 ratio are presented in Figure 2. The increase in static resting time resulted in the higher compressive strength of the steam-cured concrete, with larger growth rates observed for the demolding and 28-day compressive strength. For instance, compared to the 1-hour resting time, the demolding compressive strength of the steam-cured concrete increased by 4.29%, 9.15%, and 16.71% after static resting times of 2 h, 3 h, and 4 h, respectively. Similarly, the 28-day compressive strength increased by 12.60%, 16.80%, and 17.86%. The increase in static resting time resulted in the higher compressive strength, with larger growth rates observed for the demolding and 28-day compressive strength. The reason for this increase was that during the resting process, the concrete obtained a certain level of structural strength, which enabled it to withstand the thermal expansion damage caused by high-temperature curing and provided a solid foundation for subsequent strength growth. Based on the growth rate of compressive strength after 28 days, a static resting time of 3 h is recommended for practical engineering considerations related to efficiency and productivity.

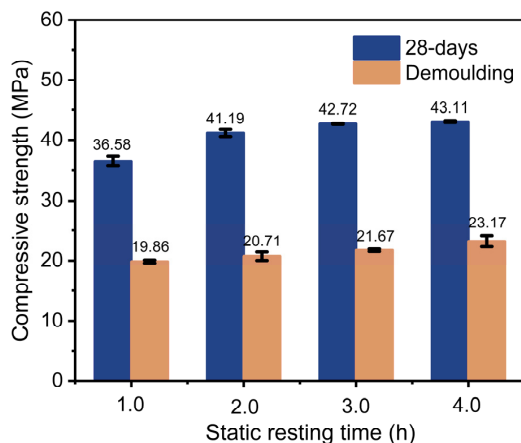


Figure 2. Concrete demolding and the influence of 28-day compressive strength with pre-curing time.

3.1.3. The Effect of Constant Temperature Time on the Compressive Strength

The constant temperature period is the main period of concrete strength growth. The study into steam-cured concrete with a mix ratio of L3 (1:1 fly ash and slag) under different steam curing constant temperature regimes shows the variation law of 1-day demolding and 28-day compressive strength in Figure 3. Compared to the constant temperature of 3 h, the demolding compressive strength of mineral concrete increased by 3.50%, 7.84%, and 14.24% after constant temperatures of 4 h, 6 h, and 8 h, respectively, while the 28-day compressive strength decreased by 1.51%, 3.64%, and 7.95%, respectively. The extension of the constant temperature period increased the demolding strength of the concrete, though it had an adverse effect on the later 28-day compressive strength. In the early stage of the hydration, high-temperature curing produced coarser new crystals, which increased the amount of coarse short fiber-shaped crystal hydration products, resulting in an increase in the 1-day demolding compressive strength. With the extension of the constant temperature period, on one hand, the high-temperature curing had a higher degree of polymerization of the silicate chains, though the water content of the binder was significantly reduced, and the microstructure of the cement paste became rougher and more porous. On the other hand, the incomplete hydration particles present in the later stage formed a blocking film to hinder hydration, the connecting points between hydration products were reduced, and the 28-day strength obtained via high-temperature curing was lower [31,45]. According to the decrease rate in 28-day compressive strength of the concrete with constant temperature time, it is known that when the steam curing constant temperature time exceeded 6 h, the rate of decrease in compressive strength increased. Therefore, the constant temperature time should be within 6 h.

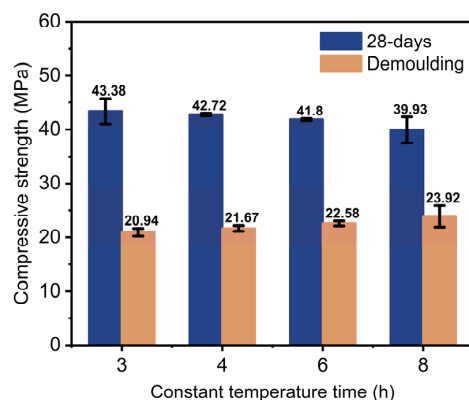


Figure 3. Effect of demolding and 28-day compressive strength in concrete with a constant temperature time.

3.2. Pore Structure

3.2.1. The Effect of Mineral Admixtures on the Pore Structure

Concrete is a complex heterogeneous multiphase material, and its pores are mainly composed of gel pores and capillary pores. Some researchers have classified the pores into four categories based on their sizes: harmless pores (<20 nm), less harmful pores (20–100 nm), harmful pores (100–200 nm), and highly harmful pores (>200 nm). Figure 4 and Table 8 show the pore volume and pore size distribution of the steam-cured concrete with varied mineral mix ratios under the same curing condition of P3. It was found that compared to the concrete that incorporated single minerals, the total porosity of the concrete with blended mineral admixtures decreased, while the proportion of harmless pores (<20 nm) increased. However, the total amount of harmful and highly harmful pores (100–200 nm and >200 nm) decreased. For instance, the single addition of fly ash was 30.4%; blended ratios of L2, L3, and L4 were 26%, 22.93%, and 27.87%; and the single incorporation of slag was 28.61%. As the slag ratio increased during the blending process, the proportion of harmless pores decreased, indicating a transition from less harmful to

harmless pores. As shown in Table 8, when blended with mineral admixture, the total porosity and proportion of highly harmful pores in the concrete with fly ash to slag ratio of 1:1 were the smallest; thus, the total amount of harmless and less harmful pores smaller than 100 nm was the largest.

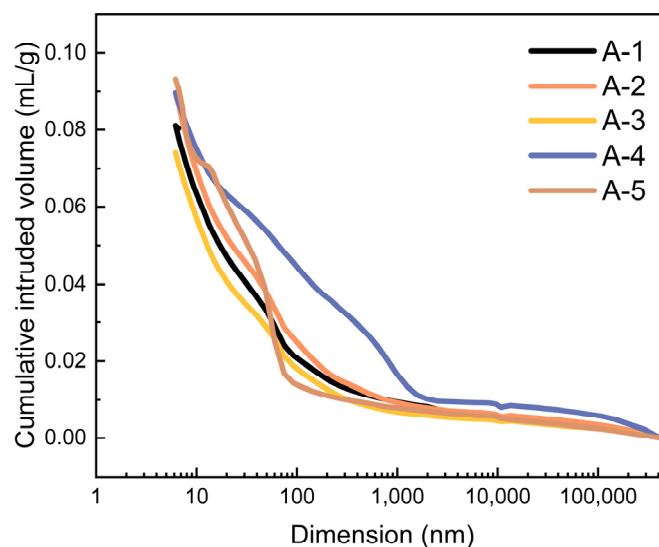


Figure 4. Different mineral admixture ratios of the relation curve of cumulative mercury and pore radius.

Table 8. P3 steam curing system's different ratio mercury porosimetry test results.

Group	Total Porosity (%)	Average Pore Diameter (nm)	Pore Size Distribution (%)			
			<20 (nm)	20–100 (nm)	100–200 (nm)	>200 (nm)
A-1	19.15	28.2	35.50	34.1	10.60	19.80
A-2	15.15	19.2	42.40	31.60	7.67	18.33
A-3	13.21	18.3	45.50	31.57	6.50	16.43
A-4	15.34	26.8	49.63	22.5	7.81	20.06
A-5	16.31	19.2	40.40	31.29	9.15	19.46

The steam-cured concrete with mineral admixtures had a reduced total porosity and increased proportion of harmless pores, and the blending of mineral admixtures can significantly improve the pore structure of the concrete. The combined effects of the blended mineral admixtures, the micro-aggregate reaction, and the active volcanic ash can reduce thermal damage; effectively reduce the high-temperature field inside the concrete; and lower the temperature stress, thus leading to finer concrete pore size and more reasonable pore size distribution. Due to their small particle size, the blended mineral admixtures can fill the voids in the cement, displace unhydrated free water, and reduce the pores formed after water evaporation. Additionally, the secondary hydration effect of the active powders effectively improved the interfacial transition zone and pore size distribution of the concrete, significantly increasing the quantity of C-S-H gel and making the interface structure more compact [31]. High-temperature curing can increase the activity of fly ash and slag and cause them to have earlier participation in reactions. As shown in Figure 4, compared to the concrete with a single mineral admixture, the concrete that incorporates blended mineral admixtures refined coarse pores in the matrix and optimized the pore structure distribution.

3.2.2. The Effect of Static Resting Time on the Pore Structure

Figure 5 and Table 9 exhibit the pore volume and pore size distribution of the steam-cured concrete with varied static resting times under the curing condition of B-1 to B-4.

It was observed that the total porosity of the steam-cured concrete decreased from 16.55 to 12.24% as the static resting time was prolonged, and the proportion of harmless pores (<20 nm) increased from 27.85 to 45.18%. The proportion of harmful pores (>200 nm) decreases, indicating a transformation from large to small pores.

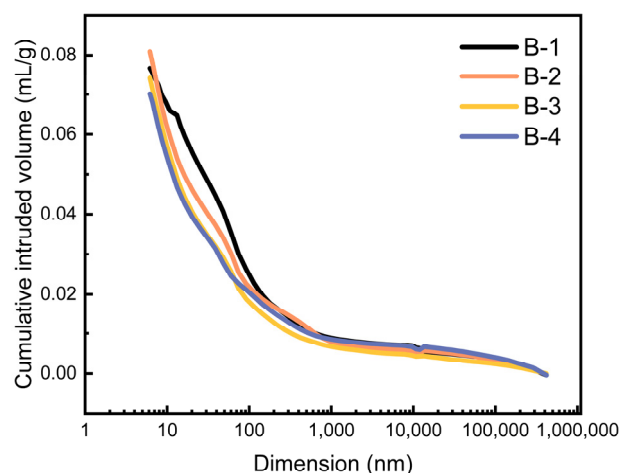


Figure 5. Different static resting times of the relation curves of cumulative mercury and pore radius.

Table 9. Test results of the mercury injection method for L3 mineral concrete with different static resting times.

Group	Total Porosity (%)	Average Pore Diameter (nm)	Pore Size Distribution (%)			
			<20 (nm)	20–100 (nm)	100–200 (nm)	>200 (nm)
B-1	16.55	16.2	27.85	42.02	8.10	22.03
B-2	14.18	18.8	43.29	31.20	5.29	20.22
B-3	13.21	18.3	45.50	31.57	6.50	16.43
B-4	12.24	18.9	45.18	31.13	7.07	16.62

The extension of static resting time had an improvement effect on the pore structure of steam-cured concrete. During the heating stage of the steam-curing process, the increase in temperature around the specimen caused water and steam in the surface layer of the specimen to expand, resulting in temperature gradients forming between the surface and the interior. This result led to uneven temperature distribution inside the concrete during the initial steam curing stage, as well as uneven migration of water and ion media and inconsistent hydration processes. Water in concrete diffused from high temperature areas to low temperature areas, resulting in two scenarios: surface moisture migrating to the interior, and water transforming into the gaseous phase. Prolonged static resting times promoted the initial strength of mineral concrete, which impeded the migration of surface moisture to the interior and the transformation of water into the gaseous phase, reduced the volume expansion caused by steam heating, and, thus, inhibited the damage caused by high-temperature steam curing to the internal pore structure of the concrete [46].

3.2.3. The Effect of Constant Temperature Time on the Pore Structure

The pore volume and pore size distribution of the steam-cured concrete with different constant temperature times under the curing conditions of C-1 to C-4 are shown in Figure 6 and Table 10. It was found that an increase in constant temperature time resulted in an increase in the porosity of the steam-cured concrete from 9.46 to 22.47%. Although the proportion of harmless pores (<20 nm) increased, the total proportion of harmful pores and highly harmful pores (>100 nm) increased from 20.59 to 26.07%. Furthermore, the total proportion of harmless and less harmful pores (<100 nm) decreased from 79.41 to 73.93%, while the proportion of highly harmful pores (>100 nm) remained relatively stable.

The proportion of harmful pores (100–200 nm) increased from 4.01 to 9.56%, indicating that the pore distribution shifted from small to large pores, while an increase in constant temperature time had an adverse effect on the pore structure.

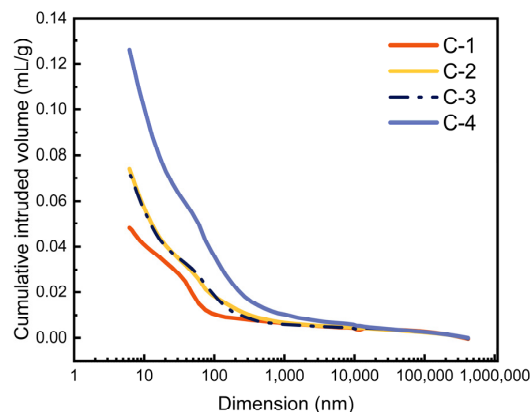


Figure 6. Different constant temperature time of the relation curves of cumulative mercury and pore radius.

Table 10. Test results of the mercury injection method for L3 mineral concrete with different constant temperature times.

Group	Total Porosity (%)	Average Pore Diameter (nm)	Pore Size Distribution (%)			
			<20 (nm)	20–100 (nm)	100–200 (nm)	>200 (nm)
C-1	9.46	23.2	48.04	31.37	4.01	16.58
C-2	13.21	18.3	45.50	31.57	6.50	16.43
C-3	12.83	18.8	44.83	30.23	8.39	16.55
C-4	22.47	19.8	42.27	31.66	9.56	16.51

A longer constant temperature time resulted in more pores being formed inside the steam-cured concrete, mainly due to the initial temperature difference between the inside and outside of the concrete during the constant temperature curing process, which generated temperature stress and an uneven temperature distribution. This result caused water to migrate inside the concrete, and with the passage of time during the constant temperature period, the temperatures inside and outside gradually reached equilibrium, causing the water inside the concrete to transform into gas [47]. Since the constant temperature-based curing process occurs at high temperatures, a longer constant temperature time can easily cause interconnected bubbles to form inside the concrete, which is more likely to damage the internal structure of the concrete. Therefore, a longer constant temperature time had an adverse effect on the pore structure of the concrete, while high-temperature curing can accelerate cement hydration and improve the early strength of the concrete.

3.3. TG-DTG Analyses

Based on the relevant literature [48,49], it is known that there are two weight loss effects related to the cement-based specimens at 400–550 °C and 600–800 °C, corresponding to the decomposition reactions of Ca(OH)_2 and CaCO_3 , respectively. Between the starting and ending points of the exothermic peak at 400–550 °C, the weight loss on the corresponding TG curve occurs due to the mass of water released from the decomposition of Ca(OH)_2 (M1), which can be calculated to determine the content of Ca(OH)_2 based on the relevant chemical equation.

The chemical equation for the decomposition of Ca(OH)_2 is shown in Equation (2):

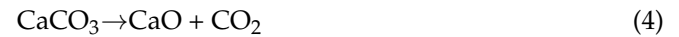


The obtained mass fraction of calcium hydroxide is denoted as $M2$:

$$M2 = 4.11 \times M1 \quad (3)$$

Between the starting and ending points of the exothermic peak within the range of 600–800 °C, the weight loss on the corresponding TG curve occurs due to the mass of CO_2 released during the decomposition of CaCO_3 , which is denoted as $M3$. The content of Ca(OH)_2 can be calculated based on the relevant chemical equation.

The chemical equation for the decomposition of CaCO_3 is:



The obtained mass fraction of Ca(OH)_2 is denoted as $M4$:

$$M4 = 1.682 \times M3 \quad (5)$$

Therefore, based on Equations (3) and (5), the total content of Ca(OH)_2 in each specimen can be obtained, as shown in Equation (6):

$$M = M2 + M4 \quad (6)$$

Figure 7 shows the TG-DTG curve of the A-1 group mortar. The calculated results of Ca(OH)_2 content for different specimens are presented in Table 11. In cement hydration products, Ca(OH)_2 is an important component that can stimulate the activity of supplementary cementitious materials, such as fly ash and slag, as well as make the hardened cement paste highly alkaline. Furthermore, Ca(OH)_2 has a direct relationship with the strength and durability of concrete.

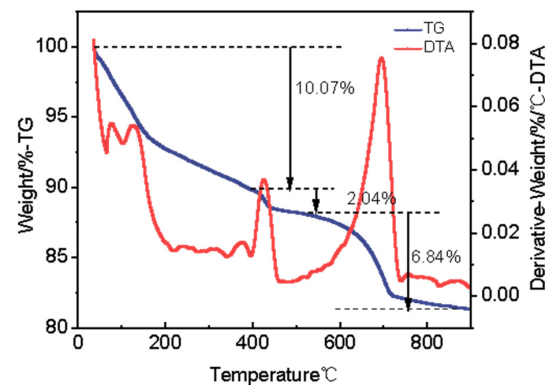


Figure 7. TG/DTG and DTA thermogravimetric curves of A1.

As shown in Table 11, the Ca(OH)_2 content in the mortar was the lowest when fly ash was used as the sole mineral admixture, because the secondary hydration of fly ash consumed Ca(OH)_2 , leading to a slow decline in its content. Compared to the use of fly ash alone, when slag was used as the sole admixture, it also underwent pozzolanic reaction in highly alkaline environments, consuming Ca(OH)_2 in the system. However, slag contains CaO , which is likely to gradually dissolve and generate Ca(OH)_2 during the pozzolanic reaction [50,51].

Therefore, when fly ash and slag were co-used, the Ca(OH)_2 content was higher than that of fly ash alone. When fly ash and slag were mixed in a ratio of 1:0.5 or 1:2, the Ca(OH)_2 content in the concrete was divided between that of fly ash alone and slag alone, which may be related to the fact that slag itself contained CaO . When fly ash and slag were mixed in equal amounts, the Ca(OH)_2 content was the highest. The reason for this finding may be that the hydration of slag and fly ash reduced the Ca(OH)_2 content in the composite system, while also promoting the complete hydration of cement, and the

Ca(OH)_2 content generated by the complete hydration of cement was much higher than the amount consumed by the mineral admixtures. The Ca(OH)_2 content increased with the prolongation of the static resting time. Compared to a resting time of 1 h, the Ca(OH)_2 content in the concrete increased by 8.34%, 16.11%, and 24.49%, respectively, at static resting times of 2 h, 3 h, and 4 h, respectively. The static resting time can make the steam-cured concrete resistant to internal damage caused by autoclaving, which was conducive to the hydration reaction of the concrete. The higher the Ca(OH)_2 content in concrete, the more complete the reaction. With the extension of the constant temperature time, the Ca(OH)_2 content in the concrete decreased. High temperature can accelerate the hydration of cementitious materials, stimulate the pozzolanic effect of mineral admixtures, and produce a secondary hydration effect, thereby consuming Ca(OH)_2 and reducing the alkalinity of the interior of mineral concrete. Compared to a static resting time of 3 h, the Ca(OH)_2 content in the concrete decreased by 10.18%, 17.88%, and 23.36%, respectively, at constant temperature times of 4 h, 6 h, and 8 h, respectively. When the constant temperature time exceeded 6 h, the trend of decreasing Ca(OH)_2 content increased. Therefore, the constant temperature time should not exceed 6 h.

Table 11. Calcium hydroxide content in the paste.

Group	Maintenance System	Fly Ash (kg/m^3)	Slag (kg/m^3)	CH Content (%)
A-1	P3	130	0	8.99
A-2	P3	86.7	43.3	11.01
A-3	P3	65	65	12.61
A-4	P3	43.3	86.7	11.89
A-5	P3	0	130	12.52
B-1	P1	65	65	10.86
B-2	P2	65	65	11.77
B-3	P3	65	65	12.61
B-4	P4	65	65	13.52
C-1	P5	65	65	14.04
C-2	P3	65	65	12.61
C-3	P6	65	65	11.53
C-4	P7	65	65	10.76

3.4. Resistance to Chloride Penetration

3.4.1. The Effect of Mineral Admixtures on the Resistance to Chloride Penetration

The relative influence of different fly ash-to-slag ratios (1:0, 1:0.5, 1:1, 1:2, 0:1) on the chloride ion permeability of the steam-cured concrete are shown in Figure 8. Compared to L1, the chloride migration coefficient of the concrete in L2 to L5 decreased by 13.53%, 23.70%, 15.69%, and 11.76%, respectively. The chloride ion resistance of the concrete with blended mineral admixtures was better than that of the concrete with single blended minerals. The best chloride ion resistance performance of the concrete was obtained when the ratio of fly ash to slag was 1:1.

Compared to the use of single-mineral admixtures, the addition of two mineral admixtures to steam-cured concrete resulted in a relatively lower chloride ion migration coefficient and better resistance to chloride ion permeability. This result occurred due to the overlapping effect of fly ash and slag, which was beneficial for improving the structure between the aggregate and the cement paste. As we described in Section 3.2, the total porosity of concrete with multiple mineral admixtures was reduced, and the proportions of harmful pores and multiple harmful pores were lower than those of the concrete with single-mineral admixtures, which increased the compactness of the concrete and enhanced its resistance to chloride ion permeability. When fly ash and slag were used in a ratio of 1:1, the hydration reaction proceeded sufficiently and they promoted each other, thus improving the compactness of the concrete. The total porosity and multiple harmful pore proportion of the

mineral admixture concrete were the smallest, resulting in the best resistance to chloride ion penetration.

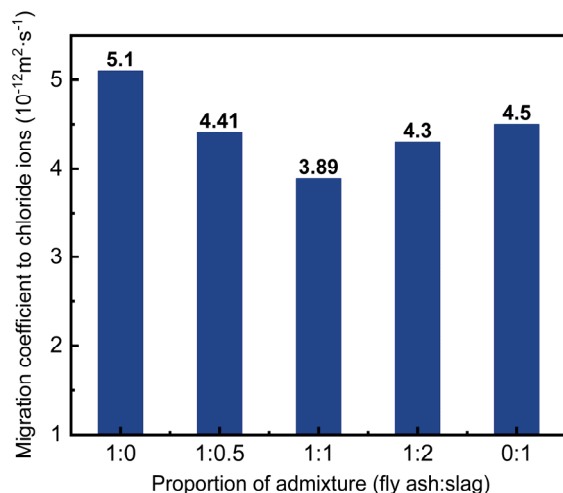


Figure 8. Effect of the compound ratio of admixture on the chloride ion transfer coefficient of the steam curing concrete.

3.4.2. The Effect of Static Resting Time on the Resistance to Chloride Penetration

The effect of different resting times on the chloride ion migration coefficient of the steam-cured concrete specimens (L1, L3, and L5) is shown in Figure 9. Compared to the resting time of 1 h, the resistance of L1 concrete to chloride ion migration decreased by 5.88%, 14.90%, and 18.24% after resting for 2, 3, and 4 h, respectively. The resistance of L3 concrete to chloride ion penetration decreased by 13.89%, 22.58%, and 26.32%, respectively, while the resistance of L5 concrete decreased by 4.09%, 17.00%, and 18.49%, respectively. As the resting time increased, the resistance of the concrete to chloride ion penetration improved. L3 concrete exhibited a relatively large decrease in the chloride ion migration coefficient, and the effect of resting time on L3 concrete was more significant. Therefore, increasing the resting time should be considered to improve the durability L3 concrete.

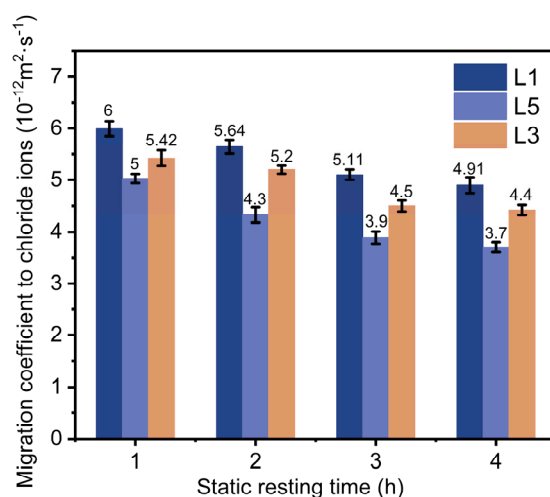


Figure 9. Effect of different static resting times on the chloride ion transfer coefficient of steam curing concrete.

According to the linear expansion coefficients of liquid, gas, and solid phases in concrete, it can be seen that the volume expansion of the solid phase is smaller than those of the liquid and gas phases. The volume expansion is mainly caused by the liquid and

gas phases. During the temperature rise process of steam curing, some of the water was converted into water vapor, which caused the increase in the porosity of the concrete. The earlier the temperature rise time, the greater the thermal expansion effect on the concrete, and the longer the static resting time, the greater the ability of the concrete to resist expansion and improve the resistance of the concrete to chloride ion penetration. As can be seen from the slope in Figure 9, when the static time was increased from 2 to 3 h, the trend of decreasing the chloride ion migration coefficient of the concrete was increased, and the decreasing trend was slowed down when the static resting time increased from 3 to 4 h. When considering the actual construction period, the static resting time should be 3 h.

3.4.3. The Effect of Constant Temperature Time on the Resistance to Chloride Penetration

The effects of different constant temperature times on the chloride ion migration coefficients of L1, L3, and L5 specimens are shown in Figure 10. Compared to the constant temperature of 3 h, the resistance of L1 specimen to chloride ion migration increased by 2.82%, 10.89%, and 12.90% at constant temperatures of 4 h, 6 h, and 8 h, respectively. The resistance of L3 specimen to chloride ion migration increased by 2.40%, 16.63%, and 28.95%, respectively, while that of L5 specimen increased by 4.65%, 20.93%, and 27.91%. As the constant temperature time increased, the resistance of the steam-cured concrete to chloride ion penetration decreased. It was also found that when the constant temperature was maintained for 3–4 h, the change in the chloride ion migration coefficient value of the concrete was relatively small. When the constant temperature was maintained for 4–6 h, the change in the chloride ion migration coefficient value of mineral concrete increased, and the rate of increase in the chloride ion migration coefficient value of the concrete also increased.

This result indicates that the resistance of concrete to chloride ion penetration decreased with the prolongation of the constant temperature time. This outcome mainly occurs because the dissolution of minerals in concrete was accelerated during the high-temperature constant temperature period. The internal molecular motion of the paste became intense, and the generation of hydration products was accelerated. Therefore, a large amount of hydration products precipitated and were disorderly overlapped, forming rough pores and increasing the structural porosity [52]. In addition, under high-temperature conditions, the expansion stress generated by moisture and air inside the concrete promoted the formation and growth of ettringite and other minerals in the microcracks between the aggregate and cement interface, making the concrete more conducive to crack development [53]. The increase in porosity and microcracks in the steam-cured concrete reduced its ability to resist chloride diffusion, leading to a decrease in its resistance to chloride ion penetration.

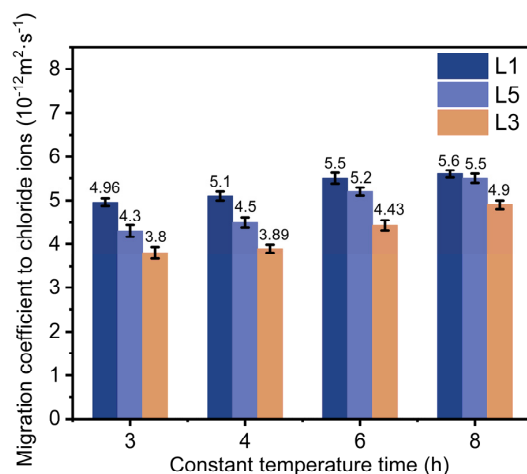


Figure 10. Effect of different constant times on the chloride ion transfer coefficient of the steam curing concrete.

4. Conclusions

This research systematically investigated the performance evolution of the concrete-incorporating minerals subjected to varied steam curing regimes by measuring their mechanical properties, permeability, and porosity. The conclusions are shown as follows:

- (1) Compared to the steam-cured concrete incorporating single minerals, the compressive strength of the concrete with both fly ash and slag was increased, the pore structure of the concrete was improved, and the alkali content was increased.
- (2) When fly ash and slag were added in equal proportions, the compressive strength and microstructure characteristics of the concrete were optimized. This outcome was attributed to the synergistic effect of the compound, which increased the compactness of the concrete and improved the interface of the cement paste and aggregates, thus contributing to the refinement of the pore structure and the compressive strength.
- (3) The extension of static resting times improved the compressive strength and microstructure of the steam-cured concrete. The improvement can be attributed to the development of structural strength in the concrete during the resting period. This enhanced structural strength enabled the concrete to withstand the detrimental effects of thermal expansion resulting from high-temperature curing, thereby establishing a firm foundation for subsequent strength development. However, a static resting time of 3 h is recommended for practical engineering considerations related to efficiency and productivity.
- (4) The extension of the constant temperature time has an adverse effect on the compressive strength, pore structure, and the content of $\text{Ca}(\text{OH})_2$ in the concrete after 28 days, though it improved the 1-day demolding strength. The constant temperature time should be controlled within 6 h.

5. Recommendations

- (1) This study only considered the influence of steam curing static resting times and constant temperature times on the durability of the concrete. Further research could be conducted into other steam curing conditions.
- (2) Due to the hydration characteristics of mineral admixtures, longer-term systematic studies can be conducted, and relevant models can be established, to provide a basis for the structural design and evaluation of durability issues related to reinforced concrete corrosion.

Author Contributions: Writing—original draft, L.W.; Investigation, W.W.; Writing—review and editing, Supervision, L.Z.; Formal analysis, J.Z.; Validation, Y.H. All authors have read and agreed to the published version of the manuscript.

Funding: This research received no external funding.

Data Availability Statement: The data presented in this study are available on request from the corresponding author.

Conflicts of Interest: The authors declare no conflict of interest.

References

1. Li, L.; Zhang, Y.; Zhou, T. Mitigation of China's carbon neutrality to global warming. *Nat. Commun.* **2022**, *13*, 5315. [[CrossRef](#)] [[PubMed](#)]
2. Abedi, M.; Rawai, N.; Fathi, M.S. Cloud Computing Information System Architecture for Precast Supply Chain Management. *Appl. Mech. Mater.* **2015**, *773–774*, 818–822. [[CrossRef](#)]
3. Agi, M.A.N.; Nishant, R. Understanding influential factors on implementing green supply chain management practices: An interpretive structural modelling analysis. *J. Environ. Manag.* **2017**, *188*, 351–363. [[CrossRef](#)]
4. Sun, Y.; Hao, S.; Long, X. A study on the measurement and influencing factors of carbon emissions in China's construction sector. *Build. Environ.* **2023**, *229*, 109912. [[CrossRef](#)]
5. Wu, G.; Yang, R.; Li, L. Factors influencing the application of prefabricated construction in China: From perspectives of technology promotion and cleaner production. *J. Clean. Prod.* **2019**, *219*, 753–762. [[CrossRef](#)]

6. Lehmann, S. Low carbon construction systems using prefabricated engineered solid wood panels for urban infill to significantly reduce greenhouse gas emissions. *Sustain. Cities Soc.* **2013**, *6*, 57–67. [[CrossRef](#)]
7. Cao, X.; Li, X.; Zhu, Y. A comparative study of environmental performance between prefabricated and traditional residential buildings in China. *J. Clean. Prod.* **2015**, *109*, 131–143. [[CrossRef](#)]
8. Hong, J.; Shen, G.-Q.; Mao, C. Life-cycle energy analysis of prefabricated building components: An input-output-based hybrid model. *J. Clean. Prod.* **2016**, *112*, 2198–2207. [[CrossRef](#)]
9. Jaillon, L.; Poon, C.S. The evolution of prefabricated residential building systems in Hong Kong: A review of the public and the private sector. *Autom. Const.* **2009**, *18*, 239–248. [[CrossRef](#)]
10. Liu, B.; Jiang, J.; Shen, S. Effects of curing methods of concrete after steam curing on mechanical strength and permeability. *Constr. Build. Mater.* **2020**, *256*, 119441. [[CrossRef](#)]
11. Yazici, H.; Yardimci, M.Y.; Aydin, S. Mechanical properties of reactive powder concrete containing mineral admixtures under different curing regimes. *Constr. Build. Mater.* **2009**, *23*, 1223–1231. [[CrossRef](#)]
12. Joesph, J.S.; Wilbur, H.C. Early Strength of Concrete as Affected by Steam Curing Temperatures. *ACI J. Proc.* **1949**, *46*, 273–283.
13. Hwang, S.D.; Khatib, R.; Lee, H.K. Optimization of steam-curing regime for high-strength, self-consolidating concrete for precast, prestressed concrete applications. *Pci. J.* **2012**, *57*, 48–62. [[CrossRef](#)]
14. Hanson, J.A. Optimum Steam Curing Procedure in Precasting Plants. *ACI J. Proc.* **1963**, *60*, 75–100.
15. Yu, N.; Chen, C.; Mahkamov, K. Selection of a phase change material and its thickness for application in walls of buildings for solar-assisted steam curing of precast concrete. *Renew. Energ.* **2020**, *150*, 808–820. [[CrossRef](#)]
16. Ma, K.; Long, G.; Xie, Y. A real case of steam-cured concrete track slab premature deterioration due to ASR and DEF. *Case Stud. Constr. Mater.* **2017**, *6*, 63–71. [[CrossRef](#)]
17. Xiang, Y.; Xie, Y.; Long, G. Volume Deformation Characteristics of Concrete Mixture during Thermal Curing Process. *MATEC Web Conf.* **2019**, *253*, 01008. [[CrossRef](#)]
18. Kim, Y.; Park, W.J.; Hanif, A. Steam-cured recycled aggregate concrete incorporating moderately high early strength cement: Effect of binder content and curing conditions. *SN Appl. Sci.* **2019**, *1*, 445. [[CrossRef](#)]
19. Wang, P.; Fu, H.; Guo, T. Volume deformation of steam-cured concrete with fly ash during and after steam curing. *Constr. Build. Mater.* **2021**, *306*, 124854. [[CrossRef](#)]
20. Long, G.; Wang, M.; Xie, Y. Experimental investigation on dynamic mechanical characteristics and microstructure of steam-cured concrete. *Sci. China Technol. Sci.* **2014**, *57*, 1902–1908. [[CrossRef](#)]
21. Zhang, Z.; Wang, Q.; Chen, H. Properties of high-volume limestone powder concrete under standard curing and steam-curing conditions. *Powder Technol.* **2016**, *301*, 16–25. [[CrossRef](#)]
22. Lothenbach, B.; Winnefeld, F.; Alder, C. Effect of temperature on the pore solution, microstructure and hydration products of Portland cement pastes. *Cem. Concr. Res.* **2007**, *37*, 483–491. [[CrossRef](#)]
23. Chen, B.; Chen, J.; Chen, X. Experimental study on compressive strength and frost resistance of steam cured concrete with mineral admixtures. *Constr. Build. Mater.* **2022**, *325*, 126725. [[CrossRef](#)]
24. Tian, Y.-G.; Li, W.-G.; Peng, B. Influence of steam-curing regimes on the freezing-thawing resistance of high strength concrete. *J. Build. Mater.* **2010**, *13*, 515–519.
25. Long, G.; He, Z.; Omran, A. Heat damage of steam curing on the surface layer of concrete. *Mag. Concr. Res.* **2012**, *64*, 995–1004. [[CrossRef](#)]
26. Ho, D.W.S.; Chua, C.W.; Tam, C.T. Steam-cured concrete incorporating mineral admixtures. *Cem. Concr. Res.* **2003**, *33*, 595–601. [[CrossRef](#)]
27. Cassagnabere, F.; Mouret, M.; Escadeillas, G. Early hydration of clinker-slag-metakaolin combination in steam curing conditions, relation with mechanical properties. *Cem. Concr. Res.* **2009**, *39*, 1164–1173. [[CrossRef](#)]
28. Erdem, T.K.; Turanli, L.; Erdogan, T.Y. Setting time: An important criterion to determine the length of the delay period before steam curing of concrete. *Cem. Concr. Res.* **2003**, *33*, 741–745. [[CrossRef](#)]
29. Xie, Y.; Wang, X.; Long, G. Quantitative analysis of the influence of subfreezing temperature on the mechanical properties of steam-cured concrete. *Constr. Build. Mater.* **2019**, *206*, 504–511. [[CrossRef](#)]
30. He, Z.; Long, G.; Xie, Y. Influence of subsequent curing on water sorptivity and pore structure of steam-cured concrete. *J. Cent. South Univ.* **2012**, *19*, 1155–1162. (In Chinese) [[CrossRef](#)]
31. Gallucci, E.; Zhang, X.; Scrivener, K.L. Effect of temperature on the microstructure of calcium silicate hydrate (C-S-H). *Cem. Concr. Res.* **2013**, *53*, 185–195. [[CrossRef](#)]
32. Shi, J.; Liu, B.; Zhou, F. Effect of steam curing regimes on temperature and humidity gradient, permeability and microstructure of concrete. *Constr. Build. Mater.* **2021**, *281*, 122562. [[CrossRef](#)]
33. Erdogdu, S.; Kurbetci, S. Optimum heat treatment cycle for cements of different type and composition. *Cem. Concr. Res.* **1998**, *28*, 1595–1604. [[CrossRef](#)]
34. Wang, M.; Xie, Y.; Long, G. The impact mechanical characteristics of steam-cured concrete under different curing temperature conditions. *Constr. Build. Mater.* **2020**, *241*, 118042. [[CrossRef](#)]
35. Liu, B.; Xie, Y.; Li, J. Influence of steam curing on the compressive strength of concrete containing supplementary cementing materials. *Cem. Concr. Res.* **2005**, *35*, 994–998. [[CrossRef](#)]

36. Yazici, H.; Aydin, S.; Yigiter, H. Effect of steam curing on class C high-volume fly ash concrete mixtures. *Cem. Concr. Res.* **2005**, *35*, 1122–1127. [[CrossRef](#)]
37. Nie, S.; Hu, S.; Wang, F. Internal curing—A suitable method for improving the performance of heat-cured concrete. *Constr. Build. Mater.* **2016**, *122*, 294–301. [[CrossRef](#)]
38. Lawrence, C.D. Mortar expansions due to delayed ettringite formation. Effects of curing period and temperature. *Constr. Build. Mater.* **1995**, *25*, 903–914. [[CrossRef](#)]
39. Shi, J.; Liu, B.; Zhou, F. Heat damage of concrete surfaces under steam curing and improvement measures. *Constr. Build. Mater.* **2020**, *252*, 119104. [[CrossRef](#)]
40. Tan, K.; Zhu, J. Influences of steam and autoclave curing on the strength and chloride permeability of high strength concrete. *Mater. Struct.* **2017**, *50*, 56. [[CrossRef](#)]
41. Ramezani-pour, A.M.; Esmaili, K.; Ghahari, S.A.; Ramezani-pour, A.A. Influence of initial steam curing and different types of mineral additives on mechanical and durability properties of self-compacting concrete. *Constr. Build. Mater.* **2014**, *73*, 187–194. [[CrossRef](#)]
42. Arshad, S.; Sharif, M.B.; Irfan-ul-Hassan, M. Efficiency of Supplementary Cementitious Materials and Natural Fiber on Mechanical Performance of Concrete. *Arab. J. Sci. Eng.* **2020**, *45*, 8577–8589. [[CrossRef](#)]
43. Peyvandi, A.; Holmes, D.; Soroushian, P. Monitoring of Sulfate Attack in Concrete by Al27 and Si29 MAS NMR Spectroscopy. *J. Mater. Civil Eng.* **2015**, *27*, 04014226. [[CrossRef](#)]
44. Zakoutsky, J.; Tydlit, V.; Cerny, R. Effect of temperature on the early-stage hydration characteristics of Portland cement: A large-volume calorimetric Study. *Constr. Build. Mater.* **2012**, *36*, 969–976. [[CrossRef](#)]
45. Elkhadiri, I.; Puertas, F. The effect of curing temperature on sulphate-resistant cement hydration and strength. *Constr. Build. Mater.* **2008**, *22*, 1331–1341. [[CrossRef](#)]
46. He, Z.-M.; Long, G.-C.; Xie, Y.-J. Surface layer degradation effect of steam-cured concrete. *J. Build. Mater.* **2014**, *17*, 994–1008.
47. Jiao, H.-Z.; Yang, W.-B.; Ruan, Z.-E.; Yu, J.-X.; Liu, J.-H.; Yang, Y.-X. The micro-scale mechanism of tailings thickening processing from metal mines. *Int. J. Miner. Metall. Mater.* **2022**, *9*, 637–650. [[CrossRef](#)]
48. Deboucha, W.; Leklou, N.; Khelidj, A. Hydration development of mineral additives blended cement using thermogravimetric analysis (TGA): Methodology of calculating the degree of hydration. *Constr. Build. Mater.* **2017**, *146*, 687–701. [[CrossRef](#)]
49. Monteagudo, S.M.; Moragues, A.; Galvez, J.C. The degree of hydration assessment of blended cement pastes by differential thermal and thermogravimetric analysis. Morphological evolution of the solid phases. *Thermochim. Acta* **2014**, *592*, 37–51. [[CrossRef](#)]
50. Jia, Y.-D. Research on Carbonation Characteristics of High Volume Mineral Admixtures Concrete. Ph.D. Thesis, Tsinghua University, Beijing, China, 2010. (In Chinese).
51. Lo, G. Effect of Curing Conditions on Carbonation Properties of Concrete with Mixed Mineral Admixture. Master's Thesis, Central South University, Changsha, China, 2014. (In Chinese).
52. Kjellsen, K.O.; Detwiler, R.J.; Gjorv, O.E. Development of microstructures in plain cement pastes hydrated at different temperatures. *Cem. Concr. Res.* **1991**, *21*, 179–189. [[CrossRef](#)]
53. Liu, W.; He, Z.-M.; Xie, Y.-J.; Xing, F. Chloride ions penetration resistance of steam curing concrete. *Concrete* **2005**, *6*, 56–60. (In Chinese)

Disclaimer/Publisher's Note: The statements, opinions and data contained in all publications are solely those of the individual author(s) and contributor(s) and not of MDPI and/or the editor(s). MDPI and/or the editor(s) disclaim responsibility for any injury to people or property resulting from any ideas, methods, instructions or products referred to in the content.